



**HAL**  
open science

## Collision induced dissociation of doubly-charged ions : Coulomb explosion vs neutral loss in $[\text{Ca}(\text{urea})]^{2+}$ gas phase unimolecular reactivity via chemical dynamics simulations.

Riccardo Spezia, Alvaro Cimas, Marie-Pierre Gaigneot, Jean-Yves Salpin,  
Kihyung Song, William L. Hase

### ► To cite this version:

Riccardo Spezia, Alvaro Cimas, Marie-Pierre Gaigneot, Jean-Yves Salpin, Kihyung Song, et al.. Collision induced dissociation of doubly-charged ions : Coulomb explosion vs neutral loss in  $[\text{Ca}(\text{urea})]^{2+}$  gas phase unimolecular reactivity via chemical dynamics simulations.. Physical Chemistry Chemical Physics, 2012, 14 (33), pp.11724-11736. 10.1039/C2CP41379E . hal-00733882

**HAL Id: hal-00733882**

**<https://hal.science/hal-00733882>**

Submitted on 31 Jan 2023

**HAL** is a multi-disciplinary open access archive for the deposit and dissemination of scientific research documents, whether they are published or not. The documents may come from teaching and research institutions in France or abroad, or from public or private research centers.

L'archive ouverte pluridisciplinaire **HAL**, est destinée au dépôt et à la diffusion de documents scientifiques de niveau recherche, publiés ou non, émanant des établissements d'enseignement et de recherche français ou étrangers, des laboratoires publics ou privés.

Cite this: *Phys. Chem. Chem. Phys.*, 2012, **14**, 11724–11736

www.rsc.org/pccp

PAPER

# Collision induced dissociation of doubly-charged ions: Coulomb explosion vs. neutral loss in $[\text{Ca}(\text{urea})]^{2+}$ gas phase unimolecular reactivity via chemical dynamics simulations†

Riccardo Spezia,<sup>\*ab</sup> Alvaro Cimas,<sup>c</sup> Marie-Pierre Gaigeot,<sup>abd</sup> Jean-Yves Salpin,<sup>ab</sup> Kihyung Song<sup>e</sup> and William L. Hase<sup>f</sup>

Received 30th April 2012, Accepted 29th June 2012

DOI: 10.1039/c2cp41379e

In this paper we report different theoretical approaches to study the gas-phase unimolecular dissociation of the doubly-charged cation  $[\text{Ca}(\text{urea})]^{2+}$ , in order to rationalize recent experimental findings. Quantum mechanical plus molecular mechanical (QM/MM) direct chemical dynamics simulations were used to investigate collision induced dissociation (CID) and rotational–vibrational energy transfer for  $\text{Ar} + [\text{Ca}(\text{urea})]^{2+}$  collisions. For the picosecond time-domain of the simulations, both neutral loss and Coulomb explosion reactions were found and the differences in their mechanisms elucidated. The loss of neutral urea subsequent to collision with Ar occurs via a shattering mechanism, while the formation of two singly-charged cations follows statistical (or almost statistical) dynamics. Vibrational–rotational energy transfer efficiencies obtained for trajectories that do not dissociate during the trajectory integration were used in conjunction with RRKM rate constants to approximate dissociation pathways assuming complete intramolecular vibrational energy redistribution (IVR) and statistical dynamics. This statistical limit predicts, as expected, that at long time the most stable species on the potential energy surface (PES) dominate. These results, coupled with experimental CID from which both neutral loss and Coulomb explosion products were obtained, show that the gas phase dissociation of this ion occurs by multiple mechanisms leading to different products and that reactivity on the complicated PES is dynamically complex.

## 1. Introduction

Doubly charged cations of metal–molecule complexes are rare and difficult to stabilize in the gas phase, but with the advent of electrospray ionization techniques they can now be generated from aqueous solutions.<sup>1</sup> While they are difficult to study in the gas phase, since most of these species are either thermochemically or kinetically unstable,<sup>2</sup> systems composed of a

divalent cation bound to a biological molecule are of great importance in biological systems.<sup>3–6</sup> Many theoretical studies have been performed to understand the structures and relative stabilities of such ion–molecule complexes, providing detailed information on the nature of their interactions and binding energies.<sup>7–13</sup> However, little is known about their reactivity. Unstable species, like  $\text{Cu}(\text{H}_2\text{O})^{2+}$ ,  $\text{Cu}(\text{NH}_3)^{2+}$  or  $\text{Pb}(\text{H}_2\text{O})^{2+}$ , have been detected in the gas phase<sup>14–16</sup> and are stabilized with long lifetimes if they are prepared in low vibrational states.<sup>17</sup> For such species containing a transition metal dication ( $\text{M}^{2+}$ ) attached to an organic base (B), a spontaneous deprotonation of the base leading to the monocation  $[\text{M}(\text{B}-\text{H})]^+$  is experimentally observed.<sup>18–21</sup> This is explained by the high recombination energy of these metal cations<sup>22</sup> (e.g. 20.3 eV for  $\text{Cu}^{2+}$  and 18.2 eV for  $\text{Ni}^{2+}$ ).  $\text{Ca}^{2+}$  has a smaller recombination energy, 12.0 eV,<sup>23</sup> and thus the corresponding  $[\text{CaB}]^{2+}$  doubly-charged species may be detected and isolated in the gas phase. Stable complexes formed by  $\text{Ca}^{2+}$  and neutral urea, glycine, thiourea, selenourea, uracil and its thio derivatives were obtained in the gas phase.<sup>24–29</sup>

These doubly-charged species can dissociate following two different processes that are in competition: a charge separation

<sup>a</sup> Université d'Evry Val d'Essonne, Laboratoire Analyse et Modélisation pour la Biologie et l'Environnement, UMR 8587 CNRS-CEA-UEVE, Bd. F. Mitterrand, 91025 Evry Cedex, France. E-mail: rspezia@univ-evry.fr

<sup>b</sup> CNRS, UMR 8587, France

<sup>c</sup> Centro de Investigação em Química, Department of Chemistry and Biochemistry, Faculty of Science, University of Porto, Rua do Campo Alegre, 687, 4169-007 Porto, Portugal

<sup>d</sup> Institut Universitaire de France, 103 Blvd St Michel, 75005 Paris, France

<sup>e</sup> Department of Chemistry, Korea National University of Education, Chungbuk, 363-791, South Korea

<sup>f</sup> Department of Chemistry and Biochemistry, Texas Tech University, Lubbock, TX 79409, USA

† Electronic supplementary information (ESI) available. See DOI: 10.1039/c2cp41379e

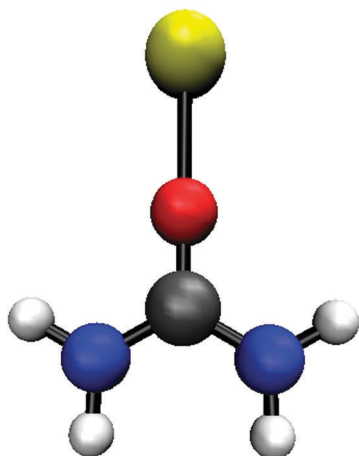


**Fig. 1** Minimum energy structure of  $[\text{Ca}(\text{urea})]^{2+}$  (11) used as the initial structure for direct dynamics simulations.

process referred to as ‘‘Coulomb explosion’’, leading to two monocations, and neutral loss fragmentation, where a new doubly-charged species, of lower mass, and a neutral molecule are obtained. The formation of the  $[\text{Ca}(\text{urea})]^{2+}$  cation (shown in Fig. 1) was recently investigated in the statistical kinetics limit.<sup>30</sup> The dissociation of  $[\text{Ca}(\text{urea})]^{2+}$  in CID has been studied by combining experiments with analysis of its potential energy surface (PES) obtained at the B3LYP level of theory.<sup>24</sup> A summary of these dissociation channels is reported in Fig. 2. Nothing has been reported regarding the detailed dissociation mechanisms and kinetics of this doubly-charged cation.

To study CID mechanisms, it is often appropriate to couple a RRKM statistical analysis<sup>31</sup> with chemical dynamics simulations<sup>32</sup> of the energy transfer in the CID experiment, with both utilizing the same PES. However, such chemical dynamics simulations often show nonstatistical dissociation mechanisms, as we recently reported for protonated urea CID.<sup>33</sup> Evidence of non-RRKM dynamics in CID has also been observed in previous experiments<sup>34</sup> and simulations<sup>35</sup> of

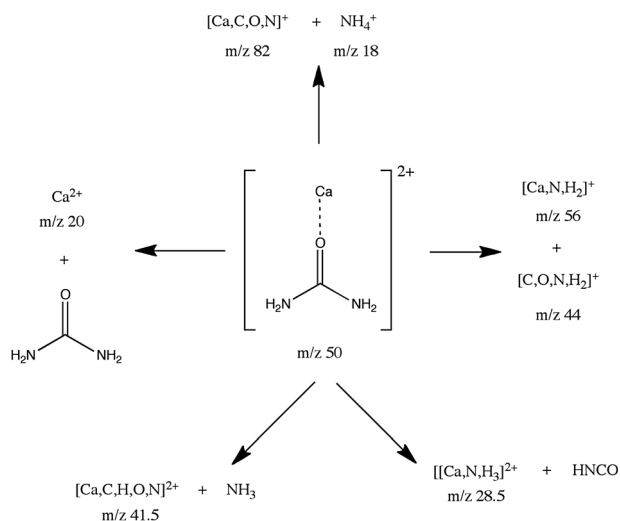


**Fig. 2** Schematic representation of the  $[\text{Ca}(\text{urea})]^{2+}$  dissociation pathways as reported by Corral *et al.*<sup>24</sup>

$\text{CH}_3\text{SH}^+ + \text{Ar}$ , experiments<sup>36</sup> and simulations<sup>37</sup> of  $\text{CH}_3\text{SCH}_3^+ + \text{Ar}$ , and simulations<sup>38,39</sup> of  $\text{Cr}^+(\text{CO})_6 + \text{Xe}$  and  $\text{H}_2\text{CO}^+ + \text{Ne}$ . Simulations suggest that nonstatistical fragmentation dynamics may also be important for CID of protonated amino acids and peptides.<sup>40,41</sup>

The goal of the present study is to investigate the different fragmentation mechanisms of a doubly charged ion. We focus on  $[\text{Ca}(\text{urea})]^{2+}$  dissociation for which both experimental CID results and an accurate PES are available,<sup>24,30</sup> pointing out, as already mentioned, that neutral losses and Coulomb explosion are possible pathways. Of interest is the competition between the different pathways and how dynamics is able to ‘‘drive’’ the dissociation. To this end, we have studied by direct dynamics simulations the short-time ps fragmentation pathways of  $[\text{Ca}(\text{urea})]^{2+}$ , focusing on collisions with Ar at 210 and 300 kcal mol<sup>-1</sup>, and comparing the simulation results with the prediction of statistical (RRKM) unimolecular rate theory. Both the simulations and RRKM calculations were performed for the same PES. Furthermore, by coupling RRKM calculations with the energy transfer efficiencies obtained from the simulations the product yields *versus* time predicted by the statistical model are found and are compared with the results of the CID simulations. An almost complete picture of the statistical *vs.* non-statistical fragmentation dynamics of  $[\text{Ca}(\text{urea})]^{2+}$  and how the different dissociation products are formed is determined.

## 2. Methods

### 2.1 PES and RRKM calculations

The  $[\text{Ca}(\text{urea})]^{2+}$  PES was investigated at the same level of theory as employed in the direct dynamics simulations, *i.e.* MP2 with the 6-31G\* basis set. Structures obtained in previous calculations, using B3LYP with the cc-pWCVTZ basis set, were used as starting structures<sup>24,30</sup> for the MP2 geometry optimizations. Zero-point energies (ZPE) were added to the resulting stationary point energies.

By using properties of minima and saddle points on the PES, quantum harmonic RRKM microcanonical rate constants were calculated as a function of internal energy and rotational quantum number  $J$ , using the standard expression:<sup>31</sup>

$$k(E, J) = \frac{\sigma N^\ddagger(E, J)}{h \rho(E, J)} \quad (1)$$

where  $\sigma$  is the reaction path degeneracy,  $N^\ddagger(E, J)$  is the sum of states of the transition state and  $\rho(E, J)$  is the density of states at the minimum. The sum and density of states were calculated using the direct count algorithm.<sup>42</sup> For the short-time dynamics considered here it is more accurate to use the quantum RRKM model than the classical RRKM model which assumes that ZPE flows freely within the molecule.<sup>43,44</sup>

Rotational effects were taken into account by considering the rotational energy for a symmetric top rotor given by

$$E_{\text{rot}}(J, K) = BJ(J + 1) + (A - B)K^2 \quad (2)$$

where  $A = \hbar^2/2I_z$ ,  $B = \hbar^2/2I_x$ ,  $J = 0, 1, 2, \dots$  and  $K = 0, \pm 1, \pm 2, \dots, \pm J$ . The symmetry axis is the  $z$ -axis and the other two

moments of inertia are  $I_x = I_y$ . For “almost symmetric tops”, where  $I_x \sim I_y$ , one can use the approximation<sup>45</sup>

$$E_{\text{rot}}(J, K) = \left( \frac{1}{I_x} + \frac{1}{I_y} \right) \frac{[J(J+1) - K^2] \hbar^2}{4} + \frac{K^2 \hbar^2}{2I_z} \quad (3)$$

The quantum number  $J$  is a constant of the motion and if  $K$  is conserved, and thus treated as adiabatic, the RRKM unimolecular rate constant for energy  $E$  and specific values of  $J$  and  $K$  is<sup>31</sup>

$$k(E, J, K) = \frac{\sigma N [E - E_0 - E_{\text{rot}}^{\neq}(J, K)]}{h \rho [E - E_{\text{rot}}(J, K)]} \quad (4)$$

where  $E_0$  is the barrier height,  $E_{\text{rot}}^{\neq}$  is the rotational energy of the transition state and  $E_{\text{rot}}$  is the same for the minimum energy structure (both obtained by eqn (3)).

The  $k(E, J)$  microcanonical rate constant, with  $K$  active, is found by averaging over  $K$  to give<sup>46</sup>

$$k(E, J) = \frac{\sigma \sum_{K=-J}^J N [E - E_0 - E_{\text{rot}}^{\neq}(J, K)]}{h \sum_{K=-J}^J \rho [E - E_{\text{rot}}(J, K)]} \quad (5)$$

We consider three situations (identified by quantum numbers  $J$  and  $K$ , each with  $K$  adiabatic) for deposition of the rotational energy on the  $[\text{Ca}(\text{urea})]^{2+}$  molecular axes. For the first case all the rotational energy is on the  $x$ - and  $y$ -axes, corresponding to  $K = 0$  and

$$J = \frac{(-1 + \sqrt{1 + 4 \frac{E_{\text{rot}}}{B}})}{2} \quad (6)$$

where  $E_{\text{rot}}$  is the rotational energy of the ion after collision and

$$\bar{B} = \left( \frac{1}{I_x} + \frac{1}{I_y} \right) \frac{\hbar^2}{4} \quad (7)$$

In the second case the rotational energy is equally distributed, such that  $E_{x,y} = 2/3 E_{\text{rot}}$  and  $E_z = 1/3 E_{\text{rot}}$ . Finally, in the third limiting case all the rotational energy is added along the  $z$ -axis so that

$$K = \sqrt{\frac{1}{3} \frac{E_{\text{rot}}}{(A - \bar{B})}} \quad (8)$$

The RRKM calculations for  $k(E, J)$ , eqn (5), and the above three models for  $k(E, J, K)$  were performed using the RRKM code by Zhu and Hase.<sup>47</sup>

In a more approximate RRKM model, for  $K$  as an active degree of freedom, the unimolecular rate constant is written as<sup>46</sup>

$$k(E, J) = \frac{\sigma N [E - E_{\text{rot}}^{\neq}(J) - E_0]}{h \rho [E - E_{\text{rot}}(J)]} \quad (9)$$

where  $N$  and  $\rho$  are written as convolutions between the densities and sums of states for the internal degrees of freedom and the active external rotation, respectively.

Finally, kinetic analyses of the statistical unimolecular dissociation of  $[\text{Ca}(\text{urea})]^{2+}$  were performed using the above RRKM rate constants and vibrational and rotational energy transfer probabilities obtained from non-reactive trajectories at the “time limit” of the chemical dynamics simulations, as done previously.<sup>33,43</sup> Structures, vibrational frequencies,

and energies of stationary points on the MP2/6-31G\* PES were used to calculate the RRKM rate constants for the different dissociation pathways. For the kinetic calculations concerning those processes where no transition structure (*i.e.* first-order saddle point) was found, we adopted the microcanonical variational transition state theory ( $\mu$ VTST) in its vibrator formulation.<sup>31,48</sup> More specifically, the potential energy paths were first scanned. Subsequently, at each point of the scan, the Hessian matrices describing the modes orthogonal to the reaction path were evaluated according to the standard procedure of Hu and Hase,<sup>49</sup> and then the sum of states was minimized to obtain the location of the loose transition state (TS). On the basis of the kinetic scheme, the steady-state solution of the master equation leads to the microcanonical expression of the overall rate coefficient:

$$k_{\text{overall}} = k_a + k_b + k_c + k_d + k_e + k_f + k_g + k_h \quad (10)$$

where the individual coefficients correspond to the different product channels (a:  $\text{Ca}^{2+} + \text{H}_2\text{NCONH}_2$ , b:  $\text{CaNH}_2^+ + \text{H}_2\text{NCO}^+$ , c:  $\text{NH}_4^+ + \text{CaNCO}^+$ , d:  $\text{NH}_4^+ + \text{CaOCN}^+$ , e:  $\text{NH}_3 + \text{CaNHCO}^{2+}$ , f:  $\text{CaNH}_3^{2+} + \text{HNCO}$ , g:  $\text{NH}_3 + \text{CaOCNH}^{2+}$ , h:  $\text{CaO}^+ + \text{H}_2\text{NCNH}_2^+$ ). The  $k$  values are given in the ESL.† These expressions were subsequently thermal averaged, according to Boltzmann distribution, in order to obtain the final canonical rate coefficients. The internal energy of the intermediates always remains equal to the collision energy plus the energy of chemical activation, where the energy of chemical activation is the relative energy of the particular intermediate with respect to the reactants (with the opposite sign).

## 2.2 Potential energy function for the CID simulations

For the CID chemical dynamics simulations the system is composed of the ion,  $[\text{Ca}(\text{urea})]^{2+}$ , and the projectile, Ar, with the total potential energy written as:

$$V = V_{\text{ion}} + V_{\text{Ar-ion}} \quad (11)$$

$V_{\text{ion}}$  is the intramolecular potential of  $[\text{Ca}(\text{urea})]^{2+}$  and it is represented by direct dynamics,<sup>50,51</sup> using the MP2/6-31G\* level of theory.  $V_{\text{Ar-ion}}$  is the interaction potential between Ar and  $[\text{Ca}(\text{urea})]^{2+}$  and was obtained from MP2/6-31G\* calculations, as done previously for the  $[\text{urea}]\text{H}^+$  chemical dynamics simulation.<sup>33</sup> For this potential we used a sum of two-body terms between Ar and the atoms of  $[\text{Ca}(\text{urea})]^{2+}$ , with each two-body term given by

$$V_{\text{Ar-ion}} = a \exp(-br) + \frac{c}{r^9} \quad (12)$$

where  $r$  is the Ar/ion-atom distance and the  $a$ ,  $b$ ,  $c$  coefficients are obtained by fitting the *ab initio* interaction potential. This potential is purely repulsive, *i.e.*  $a$  and  $c$  are always positive, as developed by Meroueh and Hase to simulate CID of protonated urea obtaining good agreement with experiments.<sup>33</sup> The same parameters of ref. 33 and 52 were used for the Ar-urea interactions. Parameters for the Ar- $\text{Ca}^{2+}$  interaction were found by fitting the Ar- $\text{Ca}^{2+}$  potential energy curve determined at the QCISD(T)/6-31++G\*\* level of theory<sup>53</sup>

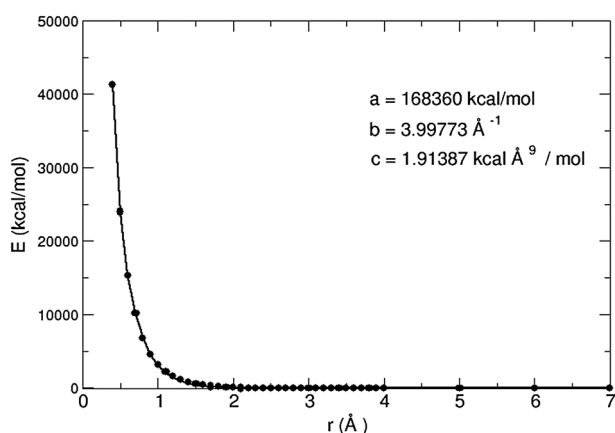


**Fig. 3** QCISD(T), circles, and fitted potential (following eqn (3)) for the Ar–Ca<sup>2+</sup> interaction potential energy curve.

(the same method as employed by Meroueh and Hase to obtain the other parameters<sup>52</sup>). BSSE correction was also taken into account following the Boys–Bernardi method.<sup>54,55</sup> The *ab initio* and fitted curves, as well as the resulting *a*, *b* and *c* parameters for the Ar–Ca<sup>2+</sup> interaction, are shown in Fig. 3. Note that we fit the curve with a purely repulsive energy function, in order to better describe the repulsive wall that is the most important feature in CID for the energies considered here. Of course, Ar–Ca<sup>2+</sup> has a shallow interaction minimum of about 2.9 Å of about 10 kcal mol<sup>−1</sup>, that can be neglected in the energy range investigated (200–300 kcal mol<sup>−1</sup>), as previously discussed by Meroueh and Hase when studying energy transfer in peptide CID.<sup>52</sup>

### 2.3 Direct dynamics trajectory simulations

The minimum energy structure, where Ca<sup>2+</sup> is bound to the urea O-atom and linear with respect to the C=O bond (see Fig. 1), was used to select initial conditions for the chemical dynamics simulations. A quasiclassical 300 K Boltzmann distribution of vibrational–rotational energies was added about the potential energy minimum.<sup>56–58</sup> Energies for the normal modes of vibration were selected from a 300 K Boltzmann distribution. The resulting normal mode energies were partitioned between kinetic and potential energies by choosing a random phase for each normal mode. A 300 K rotational energy of RT/2 was added to each principal axis of rotation. Note that the electrospray ionization source is not thermalized for experiments related to the current study. The actual temperature of ions in these experiments is surely a matter of debate. Since no precise information is available and considering that experiments are conducted in laboratories without any particular temperature control, providing an initial temperature of 300 K to the ions is probably the best choice available. This is what usually done in similar studies (see for example ref. 33, 40, 52, 63 and 65). Vibrational and rotational energies were transformed into Cartesian coordinates and momenta following algorithms implemented in VENUS.<sup>59,60</sup> The ion was then randomly rotated about its Euler angles to take into account the random directions of the Ar + [Ca(urea)]<sup>2+</sup> collisions. Relative velocities were then added to Ar + [Ca(urea)]<sup>2+</sup> in accord with the center-of-mass

collision energy and impact parameter. Collision energies of 210 and 300 kcal mol<sup>−1</sup> were considered corresponding to the experimental range.<sup>24</sup> The impact parameter, *b*, was randomly chosen between 0 and 3.0 Å. This upper value limit was chosen from geometrical considerations and inefficient energy transfer was found for larger *b*. The same value was adopted in protonated urea simulations.<sup>33</sup>

The trajectories were calculated using a software package consisting of the general chemical dynamics computer program VENUS<sup>59,60</sup> coupled to Gaussian03.<sup>61</sup> The latter was used to calculate the potential energy and gradient for the [Ca(urea)]<sup>2+</sup> intramolecular potential. The classical equations of motion were integrated using the velocity Verlet algorithm<sup>62</sup> with a time step of 0.2 fs that gives energy conservation for both reactive and nonreactive trajectories. The trajectories were initiated at an ion–projectile distance of 7.0 Å and stopped at a distance of 100.0 Å. This corresponds to a total integration time of about 1.5–2.0 ps per trajectory. A trajectory was also stopped if a reaction channel was identified. In that case a criterion distance of 7.0 Å was used to guarantee no interactions between fragments. For each simulation approximately 200 trajectories were calculated.

## 3. Results and discussions

### 3.1 PES and RRKM analysis

In Fig. 4 we schematically show the energy profile for the [Ca(urea)]<sup>2+</sup> reactions obtained at the MP2/6-31G\* level, which may be compared with the one previously reported determined using DFT (B3LYP) with a larger basis set.<sup>24,30</sup> Drawn in black are the energy levels, pathways and species that correspond to doubly-charged species and/or a neutral loss, while the ones in red correspond to Coulomb explosions. The MP2/6-31G\* calculation represents the behaviour of the PES, with only small differences in energy values as compared to the previously reported DFT PES.<sup>30</sup> In particular the products energy order is the same, providing two channels corresponding to Coulomb explosion as those with the lowest energies. Here we consider reactivity of the most stable [Ca(urea)]<sup>2+</sup> isomer, I1 following the assumed nomenclature. The energies of TS12 and I2 obtained by MP2 are slightly closer to the energy of I1 than the B3LYP ones (respective TS12 and I2 energies of 8.7 and 4.8 kcal mol<sup>−1</sup> for MP2 vs. 11.7 and 10.2 kcal mol<sup>−1</sup> for DFT). The energy of the Ca<sup>2+</sup> + urea neutral loss is similar for both methods; *i.e.* 96.3 vs. 108.3 kcal mol<sup>−1</sup> for MP2 and DFT, respectively).

The PES corresponds to the reaction scheme depicted in Fig. 5 where the rate constants, *k*'s, for each individual reaction (both forward and backward when appropriate) are also denoted. On the basis of this reaction scheme we calculated the micro-canonical rate constants that provide us information on the system dynamics in the statistical limit.

We first consider the reactivity of the reactant isomer I1 and in Fig. 6 we show the RRKM rate constants as a function of internal energy for isomerisations (*k*<sub>2</sub>, *k*<sub>11</sub>), with their corresponding backward reactions (*k*<sub>−2</sub>, *k*<sub>−11</sub>), and direct unimolecular dissociations (*k*<sub>1</sub>, *k*<sub>16</sub>) of this isomer. Here internal energies up to 300 kcal mol<sup>−1</sup> are considered. This is an upper limit for the

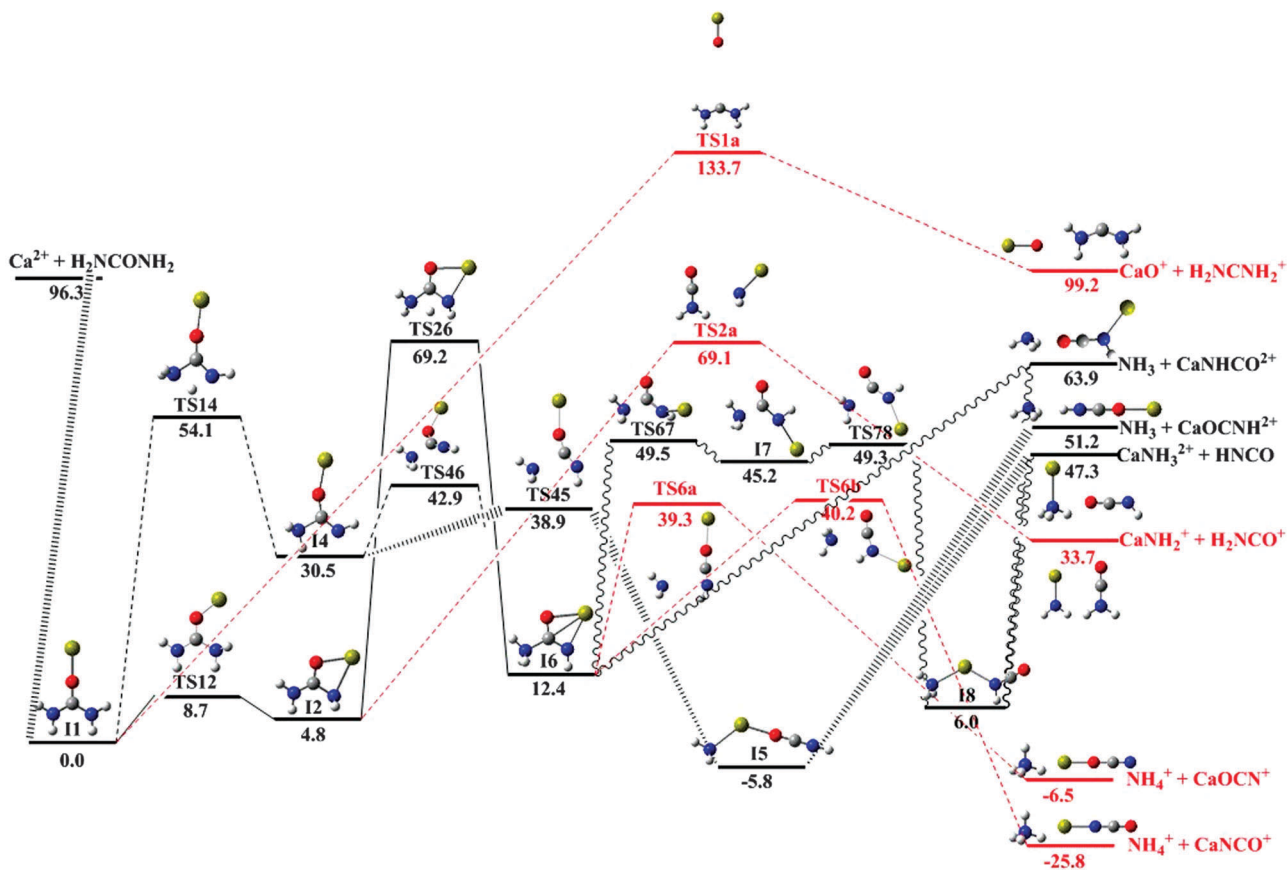


**Fig. 4** Potential energy surface for  $[\text{Ca}(\text{urea})]^{2+}$  dissociation obtained at the MP2/6-31G\* level of theory. Energies are in  $\text{kcal mol}^{-1}$ . Light (red in online version) lines correspond to Coulomb explosion pathways and products.

low collision energy regime of the CID experiments, since the energy transferred in the collision process is rarely a high percentage of the relative collision energy. From the high energy of transition state TS1a, the statistical rate constant  $k_{16}$  to form the  $\text{CaO}^+ + \text{H}_2\text{NCNH}_2^+$  products is much smaller than the other ones. Inspecting  $k_1$ ,  $k_2$  and  $k_{11}$  (*i.e.* the three remaining unimolecular rate constants for the initial structure), we see that  $k_2$  is the highest one at low energies, while  $k_1$  becomes important with increasing internal energy, crossing the  $k_2$  curve at about  $250 \text{ kcal mol}^{-1}$ . Further,  $k_{-2}$  is constantly higher than  $k_2$ , suggesting that the I2 isomer once formed from I1 can easily interconvert back to I1, while  $\text{Ca}^{2+} + \text{urea}$ , once obtained *via* the  $k_1$  pathway, cannot reform I1, since in CID experiments there is not an equilibrium between fragment and parent ions.

In Fig. 7 we show the other rate constants. What is interesting is that the  $k_3$  pathway provides reactivity in the picosecond (and shorter) time-scale for energies higher than  $150 \text{ kcal mol}^{-1}$ . This is another indication of the instability of I2 at high energy. In fact, once it is formed, it can either reform the reactants or decompose to the  $\text{CaNH}_2^+ + \text{H}_2\text{NCO}^+$  products in similar time periods. The other channel that I2 may take leads to I6. In that case the corresponding rate constant  $k_4$  is approximately two orders of magnitude smaller than  $k_3$  and  $k_{-2}$ . This  $k_4$  channel, together with the channel connecting I1 with I4, set by  $k_{11}$ , is sufficiently slow such that in the pico-second timescale we can consider it as a first-order

approximation that reactivity is confined in the region containing I1, I2 and two fragmentation products, one corresponding to a neutral loss (a product,  $m/z$  20, *i.e.*  $\text{Ca}^{2+} + \text{neutral urea}$ ) and another to a Coulomb explosion (b product,  $m/z$  56 and 44, *i.e.*  $\text{CaNH}_2^+ + \text{CONH}_2^+$ ).

On a longer time-scale the species for all product channels are formed, with a relative product yield given by the ratio of the rate constants for the two pathways. Here we qualitatively analyze the energy dependent kinetics using the RRKM  $k(E)$  for fixed  $J$  at the two limiting cases of  $J = 0$  and  $J = 80$ . More details, and in particular the role of rotational activation, are given in Section 3.4.

I4 is connected to I5 and I6 *via*  $k_{13}$  and  $k_{12}$ , respectively. Both channels are open in a sub-picosecond time-scale, and  $k_{13}$  is roughly one order of magnitude higher than  $k_{12}$ . Thus, the channel leading to I5 should be preferred. I5 can either interconvert back to I4 (*via*  $k_{-13}$ ) or give products f ( $m/z$  28.5, *i.e.*  $\text{CaNH}_3^{2+} + \text{neutral HNCO}$ ) and g ( $m/z$  41.5, *i.e.*  $\text{CaOCNH}_2^+ + \text{neutral NH}_3$ ), both corresponding to neutral loss. Note that  $k_{-13}$  increases as  $J$  increases. The reaction pathway leading to product f is much faster, such that in a first approximation the picture one can draw is that once I4 is formed it quickly isomerizes to I5 which gives a doubly-charged ion ( $\text{CaNH}_3^{2+}$ ) and a neutral molecule (HNCO), corresponding to a MS signal at  $m/z$  28.5.

If I6 is formed, then the fastest pathway leads to Coulomb explosion and products d, *i.e.* fragments  $\text{NH}_4^+ + \text{CaOCN}^+$

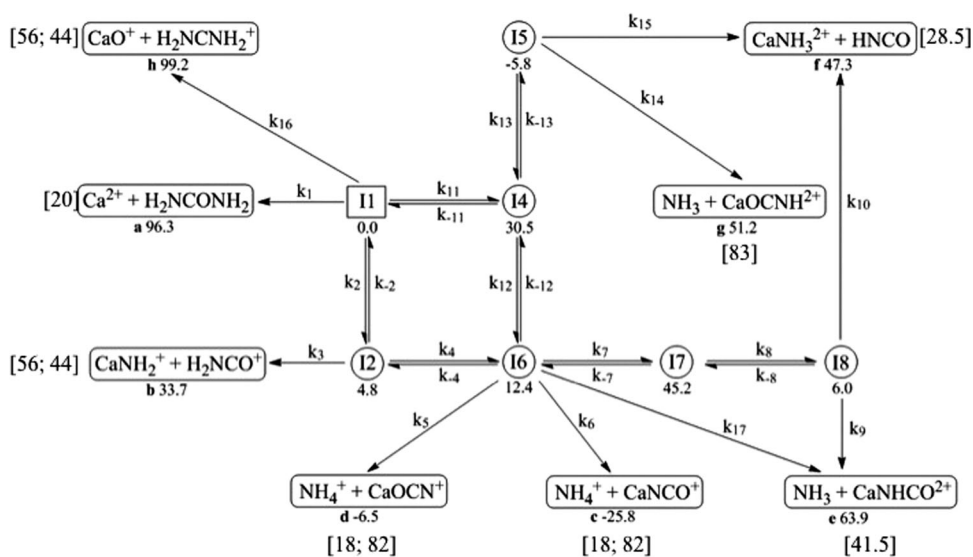


**Fig. 5** Reaction scheme corresponding to the PES of Fig. 4 with the corresponding rate constants. Relative energies (in kcal mol<sup>-1</sup>) are also shown. In brackets we report the  $m/z$  values for each fragmentation product.

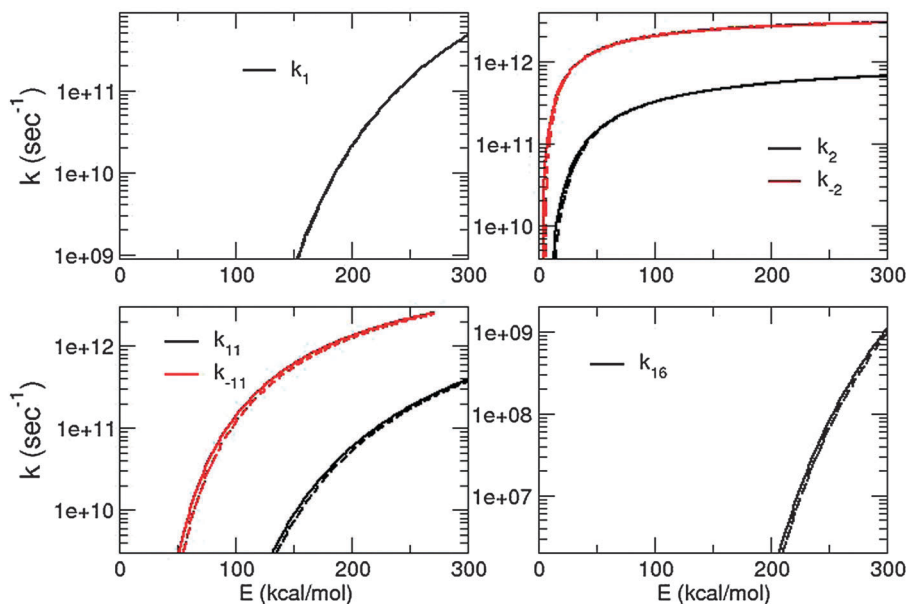


**Fig. 6** RRKM rate constants as a function of internal energy for the reactions involving direct dissociation and formation of I1. Curves for  $J = 0$  (solid lines) and  $J = 80$  (dashed lines) are shown.

( $m/z$  18 and 82 respectively). The signal corresponding to  $m/z$  41.5, that is the most intense in the reported CID spectra,<sup>24</sup> can be obtained either from product g, via the pathway connecting I1 with I4 and then I5 which can lose NH<sub>3</sub> and forming CaOCNH<sub>2</sub><sup>+</sup> (the pathway discussed above), or via I6 that can also lose NH<sub>3</sub> and forming CaNHCO<sup>2+</sup>. The kinetics of this last pathway is set by  $k_{17}$  in the sub-picosecond time-scale for collision energies higher than 100 kcal mol<sup>-1</sup>.

### 3.2 Efficiency of energy transfer

The RRKM microcanonical rate constants are a function of the energy but, as is well known, the energy transferred to vibrational and rotational motions of the ion is less than the

collision energy of the experiments (or simulations). In Fig. 8 we show the energy transferred as a function of the impact parameter,  $b$ , for the two collision energies studied in the chemical dynamics simulations. As already remarked for the energy transfer in the protonated urea CID study,<sup>33</sup> vibrational energy transfer decreases as the impact parameter increases, while the transfer to rotation slightly increases. Further, the energy transferred is smaller than the experimental collision energy by an amount that is always lower than 50% of the collision energy.

To better understand the collisional energy transfer and to use these results obtained from chemical dynamics simulations, it is important to know the probability of transferring a given amount of energy. In Fig. 9 we show the individual

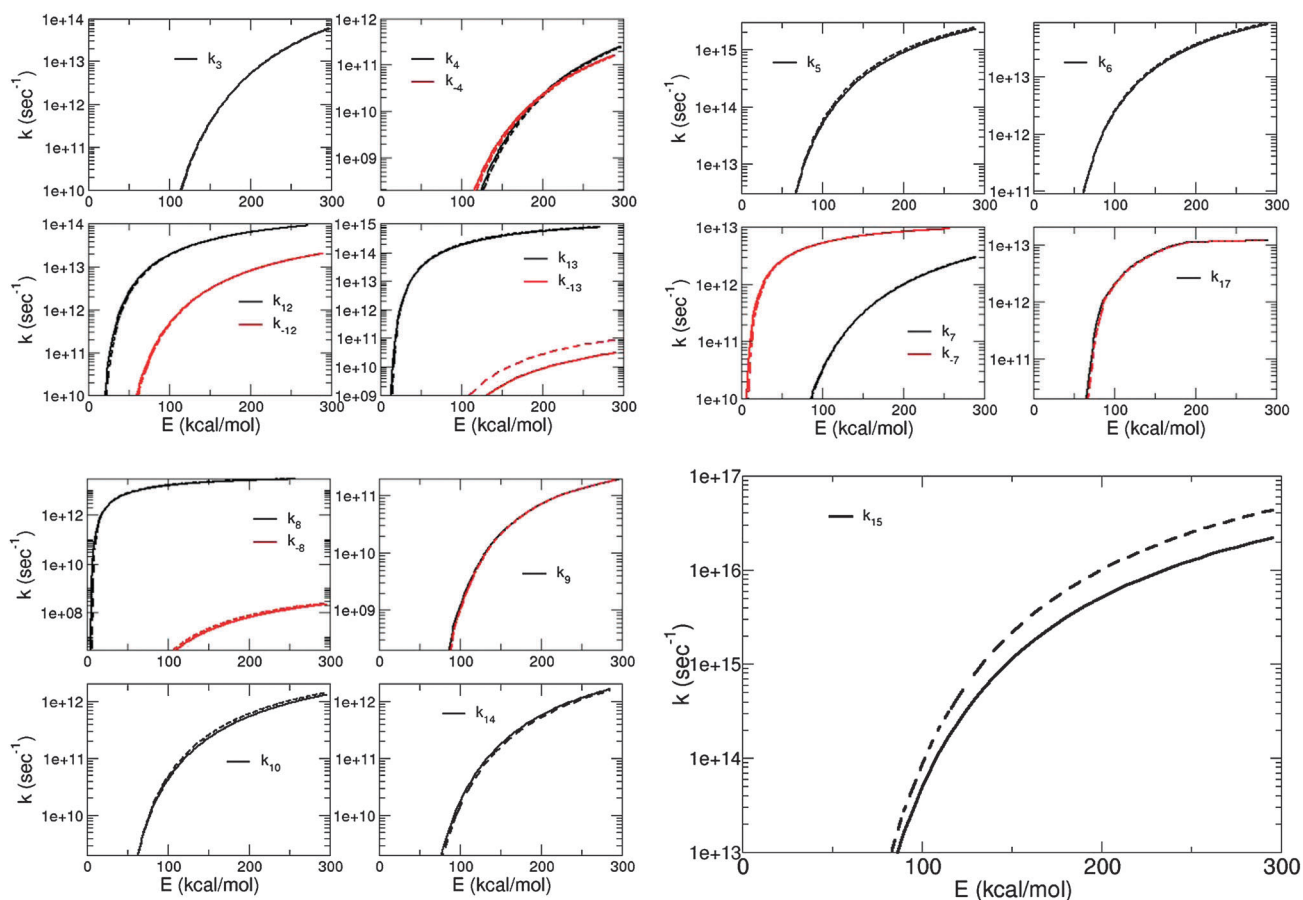


**Fig. 7** RRKM rate constants as a function of internal energy for reactions described in Fig. 5. Curves for  $J = 0$  (solid lines) and  $J = 80$  (dashed lines) are shown.

probabilities of vibrational and rotational energy transfer to  $[\text{Ca}(\text{urea})]^{2+}$ . Small energy transfers dominate and the probability goes to zero for large energy transfers. Note that a relatively high fraction of the collision energy is transferred to rotational energy, similarly to what has been found in previous simulations of the collisional activation of peptides,<sup>63</sup> planar Al clusters<sup>64</sup> and protonated urea colliding with Ar<sup>33</sup> and N<sub>2</sub>.<sup>65</sup> As expected (and shown by the results in Fig. 9) the higher is the collision energy, the higher is the probability of finding larger energy transfers. These internal energy distributions, obtained from the chemical dynamics simulations, may be combined with the RRKM rate constants to obtain a statistical analysis of the CID dynamics. We first analyze the collisions that were reactive for the time-period of the chemical dynamics simulations.

### 3.3 Dynamical reaction products and mechanisms

In Table 1 we summarize the products of the chemical dynamics simulations, identified as the species at the end of each trajectory (thus about 1.5 ps after the collision). We have identified the following  $[\text{Ca}(\text{urea})]^{2+}$  species: one with roughly the same initial structure as I1, the isomer where the C–O–Ca angle is bent (I2), and other structures where Ca<sup>2+</sup> is no longer collinear with C=O and the urea plane, but not forming isomer I2 or any other local minima on the PES shown in Fig. 4.

Reactions obtained in the time-length of our simulations correspond to the neutral loss channels, Ca<sup>2+</sup> + urea (product a,  $m/z$  20), Ca(NH<sub>3</sub>)<sup>2+</sup> + HNCO (product f,  $m/z$  28.5), and (CaNHCO)<sup>2+</sup> + NH<sub>3</sub> (product e,  $m/z$  41.5), and the Coulomb explosion, CaNH<sub>2</sub><sup>+</sup> + H<sub>2</sub>NCO<sup>+</sup> (product b, with  $m/z$  56 and 44, respectively).

The percentage of different products – those for which chemical bonds are broken and for which bonds are not broken – is both reported as a function of the collision energy in Table 1. With increasing collision energy, the probability of obtaining fragments increases from 10% to 36.5% and the probability of forming the stable  $[\text{Ca}(\text{urea})]^{2+}$  isomers I1 and I2 decreases. The probability of forming the other non-reactive isomers is largely independent of the collision energies studied. The former result comes from the destabilization of the I1 and I2 minimum energy structures when more energy is given to the system. With increasing energy there is an increase of both the neutral loss and Coulomb explosion products, with some differences discussed in the following. Before going into these details, it should be noted that at higher energy two new products Ca(NH<sub>3</sub>)<sup>2+</sup> and (CaNHCO)<sup>2+</sup> are found that are not seen at low energy, and that the Ca<sup>2+</sup> + urea neutral loss found at low energy is now four times more probable, while the Coulomb explosion pathway is two times more probable.

Results as  $m/z$  relative intensity (in %) are summarized in Fig. 10, providing “theoretical CID spectra” that can be seen

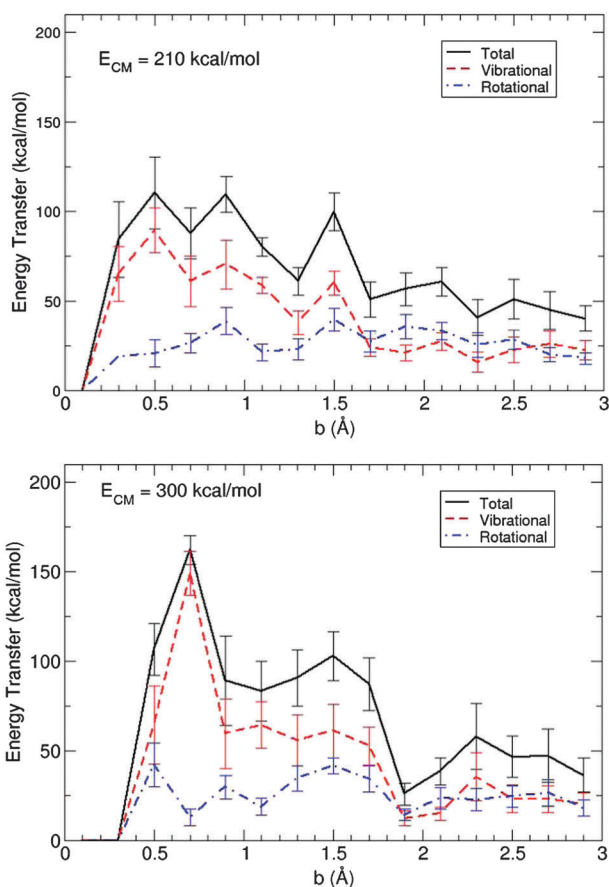


**Fig. 8** Energy transfer as a function of impact parameter. Total, vibrational, and rotational energies are shown. Uncertainties are standard deviations of the mean.

as the computational counterpart of the experimental spectra also given in Fig. 10. Comparing these spectra with the experimental low-energy CID reported previously by Corral *et al.*,<sup>24</sup> we find that in both cases the parent ion has the most intense peak ( $m/z$  50). The  $m/z$  20 peak, corresponding to neutral urea loss, is reported only as a small intensity (almost noise) peak in the experiments. This can be related to a problem in the low mass detection that can vary with the mass range chosen for quadrupole transmission, similarly to what was found recently for light fragments with the same experimental apparatus.<sup>33</sup> The other fragments corresponding to neutral loss ( $m/z$  28.5, *i.e.*  $\text{CaNH}_3^{2+}$  + neutral HNCO, and 41.5, *i.e.*  $\text{CaNHCO}^{2+}$  + neutral  $\text{NH}_3$ ), which are present with a low signal and only for high energies in the theoretical spectra, seem to be more important in the experimental spectra, in particular the  $m/z$  41.5. The two signals corresponding to Coulomb explosion ( $m/z$  44 and 56, *i.e.* paired  $\text{CONH}_2^+$  and  $\text{CaNH}_2^+$ ) are present in both experimental and theoretical spectra, with the latter having less intensity. We now describe the reaction mechanisms responsible for both the Coulomb explosion and neutral loss.

**Coulomb explosion.** Coulomb explosion gives rise to paired fragments  $m/z$  56 ( $\text{CaNH}_2^+$ ) and  $m/z$  44 ( $\text{CONH}_2^+$ ) whose intensity increases as a function of internal energy but to a less extent than neutral losses, in particular for the reaction leading to  $\text{Ca}^{2+}$ . Note that from our simulations the intensity

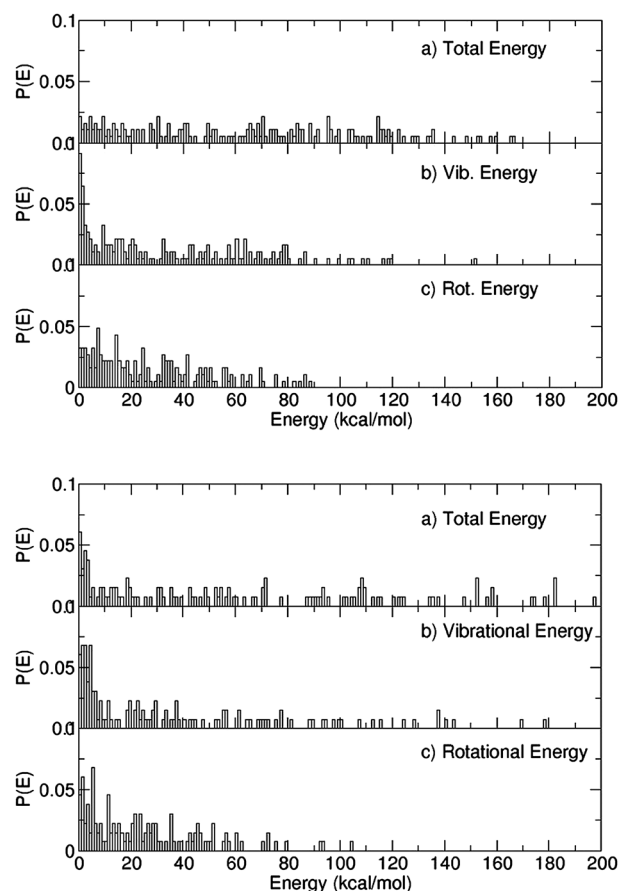


**Fig. 9** Energy transfer probabilities for  $[\text{Ca}(\text{urea})]^{2+}$  collision with Ar at two relative energies: 210 kcal mol<sup>-1</sup> (upper panel) and 300 kcal mol<sup>-1</sup> (lower panel). Total (a panels), vibrational (b panels) and rotational (c panels) energy transfers are shown.

**Table 1** Products ratio obtained from chemical dynamics simulations

	$E_{\text{coll}} = 210 \text{ kcal mol}^{-1}$	$E_{\text{coll}} = 300 \text{ kcal mol}^{-1}$
I1	45%	36%
I2	21%	4%
Other activated	23%	25%
$\text{Ca}^{2+}$ + urea	7%	29%
$\text{CaNH}_2^+$ + $\text{H}_2\text{NCO}^+$	3%	6%
$\text{Ca}(\text{NH}_3)^{2+}$ + HNCO	—	1%
$(\text{CaNHCO})^{2+}$ + $\text{NH}_3$	—	0.5%

of the two fragments is identical by definition, while in the experiments they are not exactly identical.

Looking into the details for trajectories leading to  $\text{CaNH}_2^+$  +  $\text{H}_2\text{NCO}^+$  we can identify three mechanisms. For the first, the collision activates urea rotation, weakening the Ca–O bond. As a consequence of this rotation, the  $-\text{NH}_2$  group of urea and  $\text{Ca}^{2+}$  become close and they can associate forming a singly-charged ion that dissociates due to Coulomb repulsion. This mechanism is similar to the “roundabout” mechanism recently found by Hase and co-workers in gas phase  $\text{S}_{\text{N}}2$  reactions.<sup>66</sup> A prototypical example of this reaction is given as a movie in the ESI† ( $\text{CaNH}_2$ -round.mpg). The second mechanism happens subsequent to the impact of the Ar projectile on the Ca atom of the ion. Ca migrates around urea but it has

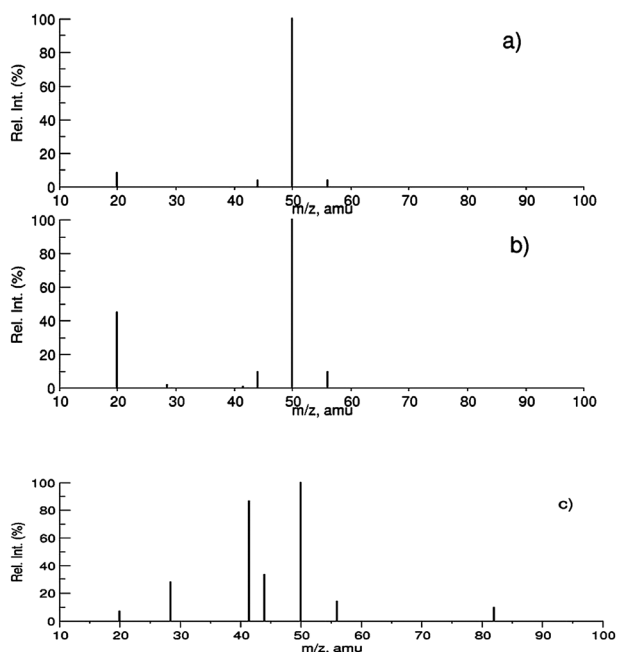


**Fig. 10** CID spectra as obtained by the chemical dynamics simulations for two collision energies: (a) 210 kcal mol<sup>-1</sup>; (b) 300 kcal mol<sup>-1</sup>. We also show in panel c experimental spectra obtained from Fig. 3 of ref. 24.

neither enough energy nor the proper direction to leave the complex. Once it reaches the -NH<sub>2</sub> group, it reacts forming the mono-cation, which then dissociates through Coulomb repulsion. An example of this “migration” mechanism is provided in the ESI† (CaNH<sub>2</sub>-moving.mpg). At low collision energy, these two mechanisms have near equal probabilities, while at high energy the roundabout mechanism is preferred.

Finally, the Coulomb explosion products can also be obtained by passing through the I2 intermediate, a mechanism that is only observed at high collision energy. The Coulomb explosion products, in the chemical dynamics simulations (see Fig. 11), are formed over a relatively long time-scale, *i.e.* in the 0.5–1.5 ps range, thus supporting the picture that this pathway is more statistically driven.

**Neutral loss.** The main neutral loss product channel is the formation of Ca<sup>2+</sup> and urea (*m/z* 20), which occurs by two

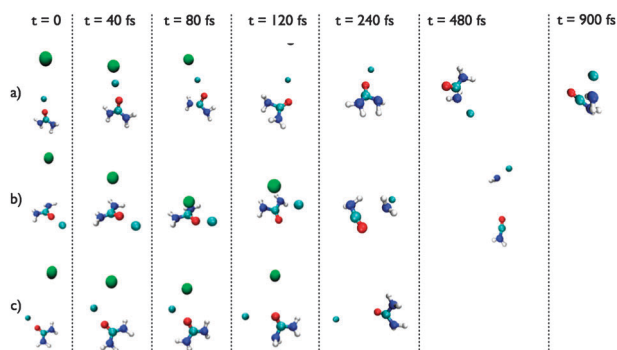


**Fig. 11** Snapshots at different simulation times for three reactive pathways: (a) Coulomb explosion with the “migration” mechanism, (b) Coulomb explosion with the “roundabout” mechanism and (c) neutral loss with the “golf-like” mechanism.

reaction mechanisms. In the first, Ar hits Ca almost perpendicular with respect to Ca–O–C, such that the shock drives Ca<sup>2+</sup> away from urea. If energy and direction are suitable, then the neutral loss is obtained with a “golf-like” mechanism. An example is reported in ESI† (Ca-golf.mpg).

Another mechanism is also responsible for the neutral loss product and formation of separated Ca<sup>2+</sup> and urea (*m/z* 20); *i.e.*, Ar strikes one of the -NH<sub>2</sub> groups, either on the opposite or lateral side with respect to Ca, with sufficient energy to detach Ca<sup>2+</sup> from neutral urea. This mechanism, noted as “side hit”, is much less frequent than the “golf-like” one. An example of this “side hit” mechanism is also given in the ESI† (Ca-side.mpg). The “golf-like” mechanism provides products in a relatively short time, 100–500 fs, while the “side hit” is a longer time process (about 400–600 fs). This supports the picture that the “golf-like” pathway is kinetically activated and is an example of a “shattering” mechanism.<sup>67,68</sup>

At low energies the “golf-like” mechanism dominates, while at higher energies the “golf-like” or “side hit” mechanisms have nearly equal probabilities. The golf-like mechanism is very dependent on the orientation of the collision and the distribution of collision orientations is, of course, independent of the collision energy. Thus, two simulations with the same number of trajectories but different collision energies, will provide roughly the same number of orientations able to give the “golf-like” mechanism. At high energy the “side hit” mechanism appears, for which Ar collides almost on the centre of [Ca(urea)]<sup>2+</sup>, activating it and leading to Ca<sup>2+</sup> dissociation.

Finally, for high energy collisions, additional channels leading to products f (*m/z* 28.5, *i.e.* CaNH<sub>3</sub><sup>2+</sup> + HNCO) and e (*m/z* 41.5, *i.e.* CaNHCO<sup>2+</sup> + NH<sub>3</sub>) occur. Both products are obtained in a short time-scale, 490 and 203 fs for f and e respectively. For f, Ca<sup>2+</sup> first migrates towards the activated -NH<sub>2</sub> group and then takes a H-atom from the other -NH<sub>2</sub> group and then the two moieties, doubly-charged CaNH<sub>3</sub><sup>2+</sup> and neutral HNCO separate. The e product is obtained in a similar way, first forming two singly-charged ions, CaNH<sub>2</sub><sup>+</sup> and H<sub>2</sub>NCO<sup>+</sup>, that stay close to each other such that NH<sub>2</sub> activated by Ca<sup>2+</sup> takes a proton from the other group, forming NH<sub>3</sub>. Now Ca<sup>2+</sup> is close enough in space to migrate to the other group, thus forming CaNHCO<sup>2+</sup>. In both cases the reactions do not clearly proceed through all the intermediates identified in the PES, and only a distorted I5 structure (with a very short lifetime) may be identified. These pathways can be considered, under the present collision conditions, dynamically activated.

In Fig. 11 we summarize the differences in activation times between Coulomb explosion (following both “migration” and “roundabout” mechanisms) and neutral loss (as an example we consider the “golf-like” mechanism). It is seen that Coulomb explosion, occurring at longer times, appears to have statistical-like dynamics, while urea loss may occur directly at short times if the collision is able to transfer sufficient energy and has the correct orientation.

### 3.4 Statistical kinetics analysis

From the distribution of collision energy transferred to the [Ca(urea)]<sup>2+</sup> ion, obtained from the chemical dynamics simulations, we can perform a microcanonical statistical analysis of

the ion's decomposition. We can consider the individual amounts of vibrational and rotational energy transferred to the ion. The latter can be particularly important when the moments of inertia of the reacting species and its transition state are very different. From our PES, as shown by the moments of inertia listed in Table S1 of the ESI†, this is the case for several of the transition states, in particular the one connecting I1 with products a, the one connecting I5 with products f via  $k_{15}$ , and TS45 with respect to I5. This is reflected by the dependence of the RRKM rate constants  $k_{15}$  and  $k_{-13}$  on  $J$ , while for  $k_1$  this effect is not evident probably because of the high energy barrier.

We thus analyze the role of treating rotational activation for  $k_{-13}$  and  $k_{15}$ , as detailed in Section 2.1. RRKM rate constants with  $K$  treated as both an adiabatic and active rotor are shown in Fig. 12. As an example, we consider a rotational energy transfer of 80 kcal mol<sup>-1</sup>. This is an upper limit of the rotational energy activation, as seen from Fig. 9, and is used in order to enhance possible rotational energy effects. When treating  $K$  adiabatically, we consider three cases of the rotational energy transfer: (i) all the energy on  $I_x$  and  $I_y$ ; (ii) an energy equally partitioned to  $I_x$ ,  $I_y$  and  $I_z$ ; and (iii) all the energy on  $I_z$ .

For  $k_{-13}$  we find that upon increasing  $K$ , with  $J$  being in a range consistent with the observed rotational energies after collision (*i.e.*  $J < 23$ ), the rate constant increases (for example  $k_{-13}(J = 14, K = 4) > k_{-13}(J = 18, K = 0)$ ). This means that the rotational energy of the reactant is higher than that of the transition state. Inspecting the moments of inertia of I5 and TS45, and their corresponding rotational constants, we have that  $B_{TS45} > B_{I5}$  and  $A_{I5} > A_{TS45}$ . The  $A$  and  $B$  rotational constants give opposite effects, with  $B$  causing a decrease in the rate constant since  $B_{TS45}J(J+1) > B_{I5}J(J+1)$ . However, the role of  $A$  is more important and it results in a larger rotational energy for I5 as compared to TS45, such that the barrier is lower and the resulting kinetics faster. Kinetics with  $J = 80$  and  $K$  treated as active, by using eqn (5), is shown in Fig. 7 and 12a and is faster than the above kinetics with smaller  $J$ . The role of the  $K$  rotational energy is emphasized by the RRKM rate constant with  $J = 80$  and  $K = 0$  (by using eqn (4)) in Fig. 12a,

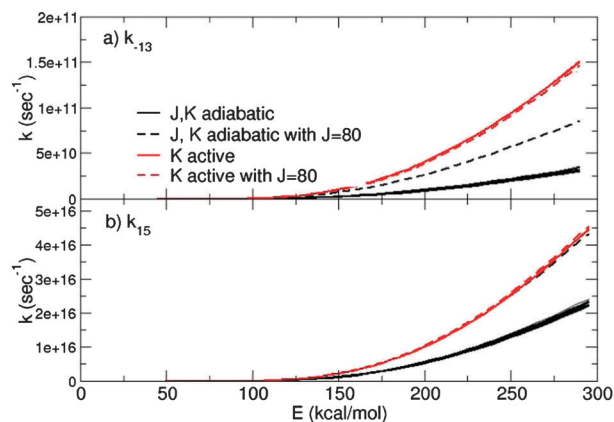


**Fig. 12** RRKM rate constants for  $k_{-13}$  and  $k_{15}$  with different treatments of rotational activation. Both  $K$  adiabatic (with different values, see text) and  $K$  as an active rotor are shown. The dashed lines highlight values for very high  $J$  (80).

which is the lowest  $k_{-13}$  for all the  $J$ ,  $K$  adiabatic curves shown. Note that  $J = 80$  corresponds to rotational energies of about 1000 kcal mol<sup>-1</sup>, that are difficult to obtain in low-energy CID experiments. Here this value is used to provide an upper limit of rotational activation. Since the reaction is greatly influenced by the  $K$  rotational quantum number, when it is treated as an active rotor we have a further increase in the  $k_{-13}$  rate constant as shown in the same Fig. 12a.

For  $k_{15}$  we note that the rate constant increases as both  $J$  and  $K$  increase, as shown in Fig. 12b, since now the  $B$  rotational constant of the transition state is smaller than that of I5 ( $B_{TS5f} < B_{I5}$ ). As above, the  $K$  active rotor has an effect to increase the rate constant and thus speed up the kinetics.

The other rate constants are not so largely affected by rotational activation. In particular, the rate constants corresponding to reactions involving I1 are not  $J$  and  $K$  dependent. Thus, in the following integrated microcanonical kinetics we will consider RRKM rate constants for I1 with only one value of  $J$  (*i.e.*  $J = 0$ , since the effect of  $J$  is negligible).

We consider reactions which are possible within a time-length that is the same (or similar) order of magnitude as for our simulations. Thus, we first restrict the full kinetic scheme to decay of I1, formation (and decay) of I2, and formation of two products: Ca<sup>2+</sup> + urea (product a, corresponding to neutral loss) and CaNH<sub>2</sub><sup>+</sup> + H<sub>2</sub>NCO<sup>+</sup> (product b, corresponding to Coulomb explosion). Note that from an analysis of the RRKM rate constants for the full reaction scheme as depicted in Fig. 5, there is a limited set of species to follow at short times due to the value of  $k_4$ , which corresponds to kinetics for a timescale much longer than the timescale accessible to the simulations. Thus, we can analyze the kinetics by using standard kinetic equations. In Fig. 13a we show the probability of  $P_a$ ,  $P_b$ , I1 and I2 as a function of time using the energy transfer probability from the chemical dynamics simulations. In the 15 ps time-scale only about 20% of the initial species react, forming mostly b products, *i.e.* Coulomb explosion with fragments CaNH<sub>2</sub><sup>+</sup>,  $m/z$  56, and H<sub>2</sub>NCO<sup>+</sup>,  $m/z$  44. I2 is initially populated since it is a transient species, while a products are never formed.

In Fig. 13b we show the statistical limit reaction kinetics corresponding to 200 kcal mol<sup>-1</sup> of energy given to the initial species. The 200 kcal mol<sup>-1</sup> of energy transferred to internal energy as vibration is an upper limit of the effectively transferred energy. For this case we now have some neutral loss within 15 ps, but the formation of neutral urea is less important than formation of two singly charged species.

In comparing the reactivity from the statistical modelling with that found from the chemical dynamics simulations, we note that the formation of products b, due to Coulomb explosion, is predominant in the statistical limit and from the dynamics it appeared that their formation seems to be more statistically driven. Importantly, the a products (neutral loss) are not found in the statistical limit and, thus, they are possible only through non-statistical reaction mechanisms, as shown in our chemical dynamics simulations.

Finally, in Table 2 we report products obtained in the canonical limit for a temperature of 300 K. We should note that here we obtain mainly species c and d, that are the most stable species in the PES and that are not obtained in

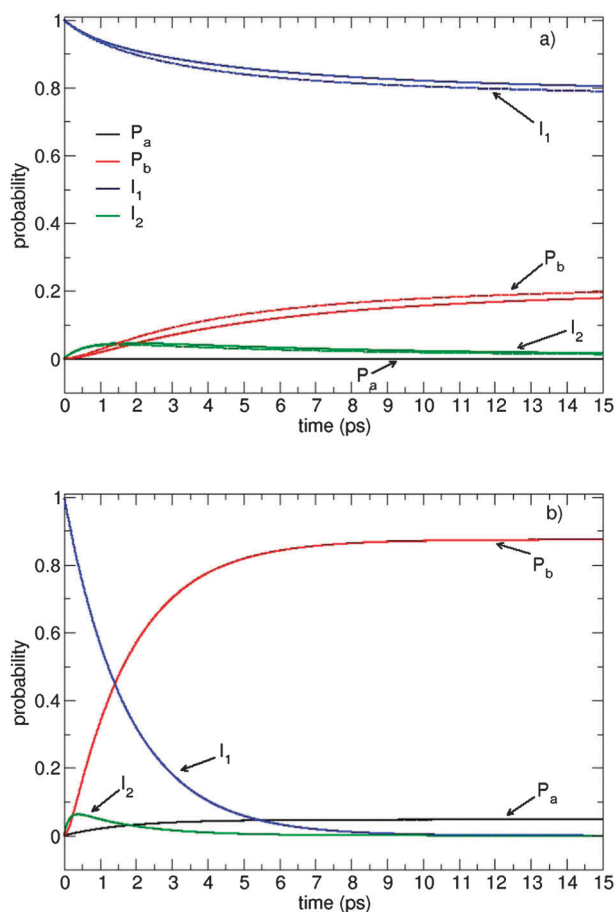


**Fig. 13** Panel a: probability of products a, b,  $I_1$  and  $I_2$  as obtained by kinetic analysis based on RRKM rate constants limited to the initial products (see text for definition), using energy transfer probabilities from the simulations with  $E_{\text{rel}} = 210 \text{ kcal mol}^{-1}$  (full lines) and  $E_{\text{rel}} = 300 \text{ kcal mol}^{-1}$  (dashed line). Panel b: the same as panel a but considering an internal energy of  $200 \text{ kcal mol}^{-1}$ .

the short-time kinetics. They are responsible for the  $m/z$  18 ( $\text{NH}_4^+$ ) and 82 peaks ( $\text{CaNCO}^+$  for c products and  $\text{CaOCN}^+$  for d products), corresponding to  $\text{NH}_4^+$  and the last being obtained in the experiments. Note that in the CID experiments the corresponding  $m/z$  18 peak is not observed with the same intensity of the  $m/z$  82 peak but, since they are coupled, this fragment should also be obtained. This may be due to the

**Table 2** Branching ratios (in %) as a function of temperature for the decomposition of the  $[\text{Ca}(\text{urea})]^{2+}$  complex in the canonical limit

$T/\text{K}$	$\text{NH}_4^+ + \text{CaNCO}^+$ (c) $m/z$ 18, 82	$\text{NH}_4^+ + \text{CaOCN}^+$ (d)	$\text{CaNH}_3^{2+} + \text{HNCO}$ (f) $m/z$ 28.5
100	99.93	0.07	0.00
150	98.32	1.68	0.00
200	72.77	27.08	0.15
250	9.18	89.57	1.25
300	8.69	89.27	2.04
350	8.33	88.80	2.87
400	7.99	88.37	3.64
450	7.68	88.00	4.31
500	7.39	87.73	4.86

experimental set-up that underestimates the intensity of low mass peaks, as reported for protonated urea<sup>33</sup> and  $[\text{Ca}(\text{urea})]^{2+}$ .<sup>24</sup> This could also be the origin of the very low signal for the  $m/z$  20 fragment corresponding to products obtained in chemical dynamics simulations. In addition, the fragment  $m/z$  28.5 (fragment f, *i.e.*  $\text{CaNH}_3^{2+} + \text{HNCO}$ ) is obtained with a low probability in the canonical kinetics limit.

## 4. Conclusions

In the present paper we studied the collision induced dissociation of a doubly-charged ion,  $[\text{Ca}(\text{urea})]^{2+}$ , for which both Coulomb explosions and neutral losses were reported by experiments.<sup>24</sup> To this end we coupled different theoretical methods: *i.e.* direct chemical dynamics simulations; analysis of RRKM rate constants on the PES used for the direct dynamics; and associated integrated microcanonical and canonical kinetics for this PES. By using these different approaches we were able to analyse different limits for the dissociation kinetics and found different dynamical behaviours for the various reaction pathways.

Product a  $\text{Ca}^{2+}$  ( $m/z$  20), corresponding to intact urea loss, is obtained as a major product in the simulations and it seems to be strongly dynamically driven. This means that it is obtained by a “shattering” mechanism and the collision orientation is a very important factor for the system to take this pathway. The high energy barrier found in the PES for this pathway basically makes this product impossible to be obtained *via* RRKM theory or a related statistical kinetic analysis for the short time scale of the simulations. Only a small peak is present in the experimental spectrum for  $m/z$  20 and shortcomings in the experimental setup may preclude an accurate measurement for this small mass to charge ratio.

The Coulomb explosion product b,  $\text{CaNH}_2^+ + \text{H}_2\text{NCO}^+$  ( $m/z$  56, 44), is obtained in both the simulations and integrated statistical kinetics in the short time limit, suggesting that an IVR mechanism drives the system towards this product channel. This is consistent with the statistical-like dynamics found for this pathway from the simulations.

The Coulomb explosion products c and d ( $m/z$  18,  $\text{NH}_4^+$ , 82,  $\text{CaNCO}^+$  or  $\text{CaOCN}^+$ ) are the most abundant fragments in the canonical limit and they are only accessible from the simulations at high collision energies. This is probably because at the lower energies the time-length available for the simulations is not sufficient for the reactive system to pass all the barriers to form these products.

The  $\text{NH}_3$  neutral losses leading to  $m/z$  41.5 (products e,  $\text{CaNHCO}^{2+}$ , and g,  $\text{CaOCNH}^{2+}$ ) are not obtained in the low energy simulations and only as minor products in the high energy simulations. Also in this case, as for the pathways leading to the c and d products, the system does not have sufficient time to pass all the barriers. Furthermore, they are less stable on the PES as compared to the c and d products. The  $\text{HNCO}$  neutral loss product f ( $m/z$  28.5) is obtained as a minor species in both the simulations at high energy and in the canonical limit.

Thus summarizing, we found that the a neutral loss pathway is primarily dynamically driven, *i.e.* the reaction happens largely before IVR takes place. The other pathways, on the other hand, seem to be obtained in different, statistical limits. In particular,

the b products are obtained in microcanonical statistical kinetics for “short” time reaction (*i.e.* several pico-seconds) and, thus, with IVR taking place. The other products are formed only at longer time scales, as found by a canonical limit analysis corresponding to an “infinite” time length.

In the following we summarize the time scales for the different reactions. In the short time scale, *i.e.* about 200 fs, the neutral loss for the high energy  $\text{Ca}^{2+} + \text{urea}$  reaction pathway dominates. In the picosecond time scale, the Coulomb explosion products for the  $\text{CaNH}_2^+ + \text{H}_2\text{NCO}^+$  reaction pathway are mainly obtained, following relatively “fast” intramolecular vibrational energy redistribution (IVR). Finally, in the long time scale, *i.e.* in the limit of the full IVR, the most stable species (*i.e.*,  $\text{NH}_4^+$ ,  $\text{CaOCN}^+$  and  $\text{CaNCO}^+$ ) dominate.

Furthermore, rotational activation of  $[\text{Ca}(\text{urea})]^{2+}$  seems to be important for some reactions, increasing the rate constant up to one order of magnitude for rotational energies available after collisions in the low-energy range. This is due to differences in moments of inertia between potential minima on the PES and transition states. For the a pathway, where such a difference is present, the corresponding rate constant does not change appreciably as a function of rotational energy (and different treatments of the *K* quantum number), probably due to the high energy barrier.

In conclusion, we have shown that the dissociation products obtained from the experiments are formed under different dynamical regimes. From the simulations it is found that a reactive system with a complex PES and different reaction pathways may have a hierarchy of complex reactivities with different dynamical limits. The short time direct dynamics show that non-statistical high energy products can be obtained before IVR takes place, whereas other product channels may be populated by IVR or more efficient collision energy transfer. The most stable products are obtained in the full thermodynamic limit.

## Acknowledgements

This work was granted access to the HPC resources of CCRT under the allocation 2011082123 made by GENCI (Grand Equipement National de Calcul Intensif). KS thanks UEVE for a visiting fellowship and partial support from the Basic Science Program through the National Research Foundation of Korea (KRF) administered by the Ministry of Education, Science and Technology (2012-0002654). AC thanks *Fundação para a Ciência ea Tecnologia* (FCT), Lisbon, Portugal. The contribution by WLH was performed as part of research supported by the National Science Foundation under Grant No. CHE-0957521 and by the Robert A. Welch Foundation under Grant No. D-0005.

## Notes and references

- P. Jayaweera, A. T. Blades, M. G. Ikonou and P. Kebarle, *J. Am. Chem. Soc.*, 1990, **112**, 2452–2454.
- D. Schröder and H. Schwarz, *J. Phys. Chem. A*, 1999, **103**, 7385–7394.
- Metal Ions in Genetic Information Transfer, Advances in Inorganic Biochemistry*, ed. G. L. Eichhorn and L. G. Marzili, Elsevier/North-Holland, New York, 1981, vol. 3.
- Metal Ions in Biological Systems: Interrelations among Metal Ions, Enzymes, and Gene Expression*, ed. A. Sigel and H. Sigel, Marcel Dekker, New York, 1989, vol. 25.
- Metal Ions in Biological Systems: Interactions of Metal Ions with Nucleotides, Nucleic Acids, and their Constituents*, ed. A. Sigel and H. Sigel, Marcel Dekker, New York, 1996, vol. 32.
- Metal Ions in Biological Systems: Probing of Nucleic Acids by Metal Ions Complexes of Small Molecules*, ed. A. Sigel and H. Sigel, Marcel Dekker, New York, 1996, vol. 32.
- E. Magnusson, *J. Phys. Chem.*, 1994, **98**, 12558–12569.
- S. Petrie, *J. Phys. Chem. A*, 2002, **106**, 7034–7041.
- G. N. Merril, S. P. Webb and D. B. Bivin, *J. Phys. Chem. A*, 2003, **107**, 386–396.
- R. Spezia, G. Tournois, T. Cartailier, J. Tortajada and Y. Jeanvoine, *J. Phys. Chem. A*, 2006, **110**, 9727–9735.
- M. Belcastro, T. Marino, N. Russo and M. Toscano, *J. Mass Spectrom.*, 2005, **40**, 300–306.
- A. Eizaguirre, O. Mó, M. Yáñez and J.-Y. Salpin, *Phys. Chem. Chem. Phys.*, 2011, **13**, 18409–18417.
- I. S. Saminathan, J. Zhao, K. W. M. Siu and A. C. Hopkinson, *Phys. Chem. Chem. Phys.*, 2011, **13**, 18307–18314.
- D. Schröder, H. Schwarz, J. Wu and C. Wesdemiotis, *Chem. Phys. Lett.*, 2001, **343**, 258–264.
- T. J. Shi, G. Orlova, J. A. Guo, D. K. Bohme, A. C. Hopkinson and K. W. M. Siu, *J. Am. Chem. Soc.*, 2004, **126**, 7975–7980.
- T. J. Shi, J. F. Zhao, A. C. Hopkinson and K. W. M. Siu, *J. Phys. Chem. B*, 2005, **109**, 10590–10593.
- A. Palacios, I. Corral, O. Mó, F. Martín and M. Yáñez, *J. Chem. Phys.*, 2005, **123**, 014315.
- S. Guillaumont, J. Tortajada, J.-Y. Salpin and A. M. Lamsabhi, *Int. J. Mass Spectrom.*, 2005, **243**, 279–293.
- N. G. Tserkezos, D. Schröder and H. Schwarz, *Int. J. Mass Spectrom.*, 2004, **235**, 33–42.
- A. M. Lamsabhi, M. Alcami, O. Mó, M. Yáñez, J. Tortajada and J.-Y. Salpin, *ChemPhysChem*, 2007, **8**, 181–187.
- W. Buchmann, R. Spezia, G. Tournois, T. Cartailier and J. Tortajada, *J. Mass Spectrom.*, 2007, **42**, 517–526.
- A. M. Lamsabhi, M. Alcami, O. Mo, M. Yáñez and J. Tortajada, *J. Phys. Chem. A*, 2006, **110**, 1943–1950.
- P. J. Linstrom and W. G. Mallard ed. NIST Chemistry Webbook. Standard Reference Database Number 69, Release June 2005, National Institute of Standards and Technology, Gaithersburg, MD, 20899, 2005.
- I. Corral, O. Mó, M. Yáñez, J.-Y. Salpin, J. Tortajada and L. Radom, *J. Phys. Chem. A*, 2004, **108**, 10080–10088.
- I. Corral, O. Mó, M. Yáñez, J.-Y. Salpin, J. Tortajada, D. Moran and L. Radom, *Chem.–Eur. J.*, 2006, **12**, 6787–6796.
- C. Trujillo, O. Mó, M. Yáñez, J.-Y. Salpin and J. Tortajada, *ChemPhysChem*, 2007, **8**, 1330–1337.
- C. Trujillo, O. Mó, M. Yáñez, J. Tortajada and J.-Y. Salpin, *J. Phys. Chem. B*, 2008, **112**, 5479–5486.
- C. Trujillo, A. M. Lamsabhi, O. Mó, M. Yáñez and J.-Y. Salpin, *Org. Biomol. Chem.*, 2008, **6**, 3695–3702.
- I. Corral, C. Trujillo, J.-Y. Salpin and M. Yáñez, in *Kinetics and dynamics: from nano- to bio-scale*, ed. P. Paneth and A. Dybala-Defratyka, Springer, 2010.
- A. Cimas, J. A. Gamez, O. Mó, M. Yáñez and J.-Y. Salpin, *Chem. Phys. Lett.*, 2008, **456**, 156–161.
- T. Baer and W. L. Hase, in *Unimolecular Reaction Dynamics – Theory and Experiments*, Oxford, New York, 1996.
- L. Sun and W. L. Hase, *Rev. Comput. Chem.*, 2003, **19**, 79–146.
- R. Spezia, J.-Y. Salpin, M.-P. Gageot, W. L. Hase and K. Song, *J. Phys. Chem. A*, 2009, **113**, 13853–13862.
- P. T. Fenn, Y.-J. Chen, S. Stimson and C. Y. Ng, *J. Phys. Chem. A*, 1997, **101**, 6513–6522.
- E. Martinez-Nunez, S. A. Vazquez and J. M. C. Marques, *J. Chem. Phys.*, 2004, **121**, 2571.
- Y.-J. Chen, P. T. Fenn, K.-C. Lau, C. Y. Ng, C.-K. Law and W.-K. Li, *J. Phys. Chem. A*, 2002, **106**, 9729–9736.
- E. Martinez-Nunez, S. A. Vazquez, E. J. Aoiz and J. F. Castillo, *J. Phys. Chem. A*, 2006, **110**, 1225–1231.
- E. Martinez-Nunez, A. Fernandes-Ramos, S. A. Vazquez, J. M. C. Marques, M. Xue and W. L. Hase, *J. Chem. Phys.*, 2005, **123**, 154311.
- J. Liu, K. Song, W. L. Hase and S. L. Anderson, *J. Chem. Phys.*, 2003, **119**, 3040.

- 
- 40 O. Meroueh, Y. Wang and W. L. Hase, *J. Phys. Chem. A*, 2002, **106**, 9983–9992.
- 41 U. Lourderaj and W. L. Hase, *J. Phys. Chem. A*, 2009, **113**, 2236–2253.
- 42 T. Bayer and D. R. Swinehart, *Commun. ACM*, 1973, **16**, 379.
- 43 G. Vayner, S. V. Addepalli, K. Song and W. L. Hase, *J. Chem. Phys.*, 2006, **125**, 014317.
- 44 U. Lourderaj, K. Park and W. L. Hase, *Int. Rev. Phys. Chem.*, 2008, **27**, 361.
- 45 C. H. Townes and A. L. Schadow, *Microwave Spectrometry*, McGraw-Hill, New York, 1955.
- 46 L. Zhu and W. L. Hase, *Chem. Phys. Lett.*, 1990, **175**, 117–124.
- 47 L. Zhu and W. L. Hase, *QCPE*, 1994, **14**, 644.
- 48 B. C. Garrett and D. G. Truhlar, *J. Chem. Phys.*, 1979, **70**, 1593.
- 49 X. Hu and W. L. Hase, *J. Chem. Phys.*, 1991, **95**, 8073.
- 50 J. Liu, K. Song, W. L. Hase and S. L. Anderson, *J. Chem. Phys.*, 2003, **119**, 3040.
- 51 W. L. Hase, K. Song and M. S. Gordon, *Comput. Sci. Eng.*, 2003, **5**, 36–44.
- 52 O. Meroueh and W. L. Hase, *J. Phys. Chem. A*, 1997, **103**, 3981–3990.
- 53 J. A. Pople, M. Head-Gordon and K. Raghavachari, *J. Chem. Phys.*, 1987, **87**, 5968.
- 54 S. F. Boys and F. Bernardi, *Mol. Phys.*, 1970, **19**, 553.
- 55 S. Simon, M. Duran and J. J. Dannenberg, *J. Chem. Phys.*, 1996, **105**, 11024.
- 56 S. Chapman and D. L. Bunker, *J. Chem. Phys.*, 1975, **62**, 2890.
- 57 C. S. Sloane and W. L. Hase, *J. Chem. Phys.*, 1977, **66**, 1523.
- 58 Y. J. Cho, S. R. Vande Linde, L. Zhu and W. L. Hase, *J. Chem. Phys.*, 1992, **96**, 8275.
- 59 X. Hu, W. L. Hase and T. Pirraglia, *J. Comput. Chem.*, 1991, **12**, 1014–1024.
- 60 W. L. Hase, R. J. Duchovic, X. Hu, A. Komornicki, K. F. Lim, D.-H. Lu, G. H. Peslherbe, K. N. Swamy, S. R. Vande Linde, A. Varandas, H. Wang and R. J. Wolf, *QCPE*, 1996, **16**, 671.
- 61 M. J. Frisch, *et al.*, *Gaussian 03, revision D.01*, Gaussian, Inc, Wallingford, CT, 2004.
- 62 W. C. Swope, H. C. Andersen, P. H. Berens and K. R. Wilson, *J. Chem. Phys.*, 1982, **76**, 637.
- 63 O. Meroueh and W. L. Hase, *Int. J. Mass Spectrom.*, 2000, **201**, 233–244.
- 64 P. de Sainte Claire, G. H. Peslherbe and W. L. Hase, *J. Phys. Chem.*, 1995, **99**, 8147–8161.
- 65 Y. Jeanvoine, M.-P. Gaijeot, W. L. Hase, K. Song and R. Spezia, *Int. J. Mass Spectrom.*, 2011, **308**, 289–298.
- 66 J. Mikosch, S. Trippel, C. Eichhorn, R. Otto, U. Lourderaj, J. X. Zhang, W. L. Hase, M. Weidemüller and R. Wester, *Science*, 2008, **319**, 183–186.
- 67 D. G. Schultz and L. Hanley, *J. Chem. Phys.*, 1998, **109**, 10976.
- 68 T. Raz and R. D. Levine, *J. Chem. Phys.*, 1996, **105**, 8097.